Figures and tables

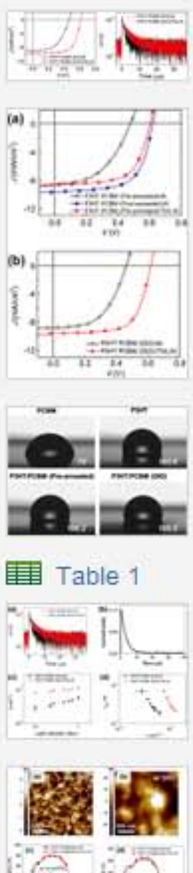

Table 1

ELSEVIER

Organic Electronics

Volume 14, Issue 7, July 2013, Pages 1749–1754

Transient photovoltage and dark current analysis on enhanced open-circuit voltage of polymer solar cells with hole blocking TiO_2 nanoparticle interfacial layer

Youn-Su Kim[a, b, c], Taehee Kim[a], BongSoo Kim[a], Doh-Kwon Lee[a], Honggon Kim[a], Byeong-Kwon Ju[b], Kyungkon Kim[c]

Show more

http://dx.doi.org/10.1016/j.orgel.2013.04.016

Highlights

- V_{OC} of additive process polymer solar cell was restored 0.46–0.62 V by inserting TiO_2 nanoparticle inter -layer (TNL).
- Photo-voltage transient reveals the TNL layer effectively suppresses charge carrier recombination at the interface.
- Solar cells having TNL shows enhanced air-stability as compared to that having Ca/Al electrode.

Abstract

The open-circuit voltage of bulk heterojunction polymer solar cells utilizing 1,8-diiodooctane (DIO) as a processing additive was greatly improved by using an organic layer coated TiO_2 nanoparticle interfacial layer inserted between the active layer and the Al electrode. The transient photovoltage measurement revealed that there was significant non-geminate recombination at the DIO-processed active layer/Al electrode interface. Reduced open-circuit voltage (V_{OC}) of the photovoltaic devices and high water contact angle of the DIO-processed active layer showed that the DIO-processed active layer has an undesirable surface composition for the electron collection. The organic layer coated TiO_2 nanoparticle interfacial layer

Organic Electronics 14 (2013) 1749–1754

Contents lists available at SciVerse ScienceDirect

Organic Electronics

journal homepage: www.elsevier.com/locate/orgel

Transient photovoltage and dark current analysis on enhanced open-circuit voltage of polymer solar cells with hole blocking TiO_2 nanoparticle interfacial layer

Youn-Su Kim [a,b,c], Taehee Kim [a], BongSoo Kim [a], Doh-Kwon Lee [a], Honggon Kim [a], Byeong-Kwon Ju [b], Kyungkon Kim [c,*]

[a] Photo-Electronic Hybrids Research Center, Korea Institute of Science and Technology (KIST), Hwarangno 14-gil, Seongbuk-gu, Seoul 136-791, Republic of Korea
[b] Display and Nanosystem Laboratory, College of Engineering, Korea University, Seoul 136-713, Republic of Korea
[c] Department of Chemistry and Nano Science, Global Top5 Research Program, Ewha Womans University, Seoul 120-750, Republic of Korea

ARTICLE INFO

Article history:
Received 27 June 2012
Received in revised form 4 April 2013
Accepted 5 April 2013
Available online 24 April 2013

Keywords:
Polymer solar cells
Transient photovoltage
Vertical phase separation
Processing additive

ABSTRACT

The open-circuit voltage of bulk heterojunction polymer solar cells utilizing 1,8-diiodooctane (DIO) as a processing additive was greatly improved by using an organic layer coated TiO_2 nanoparticle interfacial layer inserted between the active layer and the Al electrode. The transient photovoltage measurement revealed that there was significant non-geminate recombination at the DIO-processed active layer/Al electrode interface. Reduced open-circuit voltage (V_{OC}) of the photovoltaic devices and high water contact angle of the DIO-processed active layer showed that the DIO-processed active layer has an undesirable surface composition for the electron collection. The organic layer coated TiO_2 nanoparticle interfacial layer effectively prevented the non-geminate recombination at the active layer/Al interface. As a result, we were able to significantly improve the V_{OC} and power conversion efficiency from 0.46 V and 2.13% to 0.62 V and 3.95%, respectively.

1. Introduction

Polymer solar cells (PSCs) with bulk-heterojunction (BHJ) active layers consisting of conjugated polymers and fullerene derivatives have attracted keen attention as a promising future photovoltaic technology due to low-cost manufacturing, easy processability, and mechanical flexibility [1–3]. There have been tremendous attempts to improve the power conversion efficiency (PCE) of the PSCs by engineering interfacial properties as well as controlling the active morphology. For controlling the morphology of the active layer, a simple technique using processing additives was proposed [4–10]. The processing additives added into the active solution can assist the crystallization of polymer chains and the suitable formation of fullerene domains to develop interpenetrated networks [5–7]. However, Yang et al. has reported that polymer-enrichment could occur at the air surface due to the vertical phase separation of poly (3-hexylthiopene) (P3HT) and [6,6]-phenyl-C_{61}-butyric acid methyl ester (PCBM) within the BHJ active layer when processing additives were applied [11]. This vertical phase separation indicates that the conventional device configuration would be undesirable to collect electrons at the metal cathode. Notwithstanding, high PCE exceeding 4% can be obtained in the conventional device with an additive-processed active layer [9–13]. To obtain this high efficiency in previous reports, low work function metals such as Ca or LiF have been requisitely employed in order to apply a high electric field and improve the charge extraction. However, low work function metal can be easily oxidized in air. Thus, a novel material that can simultaneously minimize the charge collection loss and secure air stability is necessary. TiO_x is one of the materials which meet above requirements. The TiO_x has been applied as

* Corresponding author. Tel.: +82 02 3277 3429; fax: +82 2 3277 6766.
E-mail address: kimkk@ewha.ac.kr (K. Kim).

1566-1199/$ - see front matter © 2013 Elsevier B.V. All rights reserved.
http://dx.doi.org/10.1016/j.orgel.2013.04.016

versatile material serving as electron transporter/hole blocker, optical spacer and oxygen barrier [14,15]. Although the TiO_x is promising material for interfacial layer, the sol–gel process to prepare TiO_x layer involves hydrolysis procedure in the air which can complicates the device fabrication and causes the active material degradation. Previously, we have utilized an organic layer coated nano-crystalline TiO_2 nanoparticle, which has high dispersity and an excellent film form property compared to commercially available TiO_2 nanoparticles [16,17]. The pre-synthesized TiO_2 nanoparticle is not only solution-processable without post treatment such as hydrolysis or sintering but is also chemically stable. In this regard the nanocrystalline TiO_2 nanoparticle can be better candidate material than the TiO_x for the interfacial layer.

In this study, we show that the correlation between the reduced open-circuit voltage (V_{OC}) of the additive-processed device and the unfavorable surface composition. In addition, we demonstrate that a TiO_2 nanoparticle interfacial layer (TNL) inserted between the active layer and the metal electrode (Al) significantly reduces the charge carrier recombination and enhances the V_{OC}. This approach led to a considerable improvement in photovoltaic performance as well as in the air stability of the devices. The origin of the improvement in V_{OC} was verified by a transient photovoltage (TPV) measurement and a dark current analysis.

2. Experimental

The devices were fabricated with the conventional device configuration of ITO/poly(3,4-ethylenedioxythiophene):poly(styrenesulfonate) (PEDOT:PSS)/P3HT:PCBM/Electrode. The electrode can be Al, TNL/Al, or Ca/Al. The PEDOT:PSS (CLEVIOS™ AI 4083) layer (30 nm) was deposited by spin-coating at 4000 rpm on top of the ITO substrate and subsequently dried at 110 °C for 10 min. Then, the active layer (100 nm) was deposited by spin-coating onto the PEDOT:PSS layer. The active solutions were prepared by blending P3HT and PCBM with 1:0.8 weight ratio in chlorobenzene and 3 vol% of 1,8-diiodooctane (DIO) was added into an active solution. The TiO_2 nanoparticle interfacial layer (20 nm) was formed onto the active layer by spin-coating at 4000 rpm from the organic layer coated TiO_2 nanoparticles dispersed in ethanol (0.4 wt%). The synthesis process for the TiO_2 nanoparticles can be found in [16,18]. Finally, Al (100 nm) or Ca (20 nm)/Al (100 nm) electrode was thermally evaporated under a vacuum of 2×10^{-6} Torr. No further thermal annealing process was applied for the device with a processing additive. For the comparison, devices without the additive were prepared and the active layers were thermally annealed at 150 °C for 10 min in a vacuum chamber before or after Al evaporation. Current density versus voltage (J–V) curves were measured by a Keithley 2400 source meter under AM 1.5G irradiation (100 mW cm^{-2}) from a Xenon lamp based solar simulator (ORIEL). For the comparison of air stability between Ca/Al and TNL/Al electrode, devices were stored at a 55% of humidity and a 28 °C of temperature in the dark for stability test and they were not encapsulated.

Shuttle et al. studied charge carrier decay in P3HT:PCBM solar cell and we followed their procedure for the TPV and transient photocurrent (TPC) measurement of the above devices [19]. Detailed experimental conditions and theoretical background can be found in the paper. Briefly, the TPV and transient photocurrent (TPC) measurements were performed at steady state under continuous and variable illumination from a solar simulator with ND filter. When the device output reached a steady state, the device was perturbed using an Nd-YAG 532 nm pulsed laser (pulse rate ~1 Hz). The resulting voltage transient was acquired by a TDS3054B Tektronix digital oscilloscope with the 1 MΩ input impedance. TPV results were fitted to a mono exponential decay function in order to find the carrier recombination lifetime. TPC measurements were employed in the short circuit condition and output signal is measured using digital oscilloscope.

3. Results and discussion

Fig. 1a compares the photovoltaic performance of thermally annealed devices before (pre-annealed) or after (post-annealed) the Al electrode deposition. It is noteworthy that the pre-annealed and post-annealed devices yielded a considerable difference in V_{OC} depending on the annealing sequence in spite of the same annealing temperature and annealing time (at 150 °C for 10 min). In Fig. 1b, the device processed with 1,8-diiodooctane (DIO-processed device) presented analogous photovoltaic performance to that of the pre-annealed device. The reduced V_{OC}s in the pre-annealed and DIO-processed devices could be ascribed to the fact that the unfavorable surface composition of the active layer was induced by vertical phase separation. Considering the surface energy in thin film geometry, it is highly probable that the phase separation of P3HT and PCBM proceeds in the vertical direction as

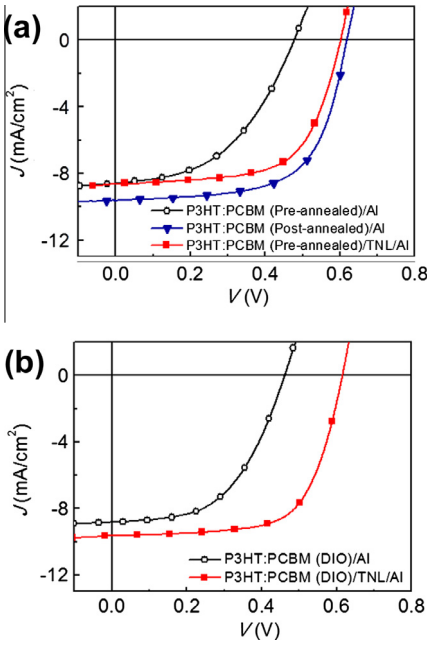

Fig. 1. J–V curves of thermally-annealed (a) and DIO-processed (b) P3HT:PCBM devices measured under illumination.

well as the lateral aspect. When the bottom and top surfaces of the P3HT:PCBM active layer are adjacent to the hydrophilic PEDOT:PSS (surface energy of 47 mN/m) [20] and the hydrophobic free surface, respectively, the P3HT phase with relatively low surface energy (26.9 mN/m) [20] preferentially segregates at the free surface, whereas the PCBM phase with higher surface energy (38.2 mN/m) [21] preferentially segregates at the active layer/PEDOT:PSS interface upon thermal annealing or upon the DIO-process. The vertical phase separation was investigated by dynamic secondary ion mass spectroscopy (DSIMS) and X-ray photoelectron spectroscopy (XPS) in previous studies [22,23]. Here, we have measured the water contact angle of the active layer with the different processing conditions as shown in Fig. 2 in order to investigate surface composition of the films. Pure P3HT and PCBM films exhibited contact angles of 105.6° and 79°, respectively. These values imply that the PCBM has a higher surface energy and a more hydrophilic nature resulting from polar ester group of the PCBM. Contact angles of pre-annealed P3HT:PCBM film (106.2°) and DIO-processed P3HT:PCBM film (105.5°) were very close to that of the pure P3HT films, indicating that P3HT-rich regions are formed at the air surface. In the conventional PSC device configuration, the polymer enrichment near the Al electrode is undesirable because the electron collection from PCBM to the Al electrode is hindered by the P3HT phase and the charge recombination should occur at the P3HT/Al interface. In other words, the unfavorable vertical phase separation of the active layer would deteriorate the charge collection efficiency and the V_{OC} of the devices [22]. In order to suppress the charge recombination and enhance the V_{OC}, we introduced a TiO_2 nanoparticle interfacial layer (TNL) as a hole blocker at the P3HT/Al interface [24,25]. When the TNL was applied to the pre-annealed and DIO-processed devices having the unfavorable surface composition, the photovoltaic performances of the pre-annealed and DIO-processed devices were significantly enhanced as shown in Fig. 1a and b. Especially, the V_{OC} and PCE of the DIO-processed device were enhanced from 0.46 V and 2.13% to 0.62 V and 3.95%, respectively. The photovoltaic parameters of Fig. 1 are listed in Table 1. This improvement regarding the photovoltaic performance can be attributed to reduced recombination at the interface between the active layer and Al.

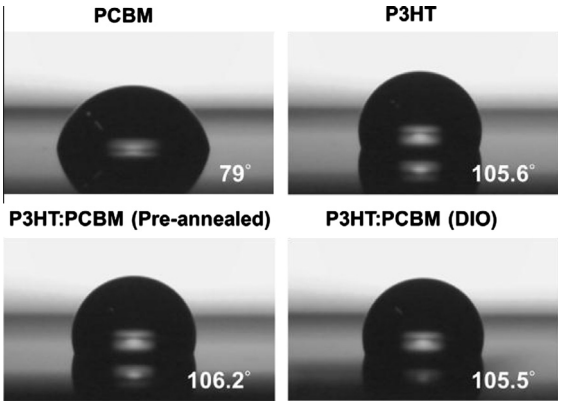

Fig. 2. Water contact angles for the pure PCBM, pure P3HT, pre-annealed P3HT:PCBM, and DIO-processed P3HT:PCBM films.

In order to corroborate the suppressed charge recombination with the TNL for the DIO-processed device, we carried out transient photovoltage (TPV) measurements. The TPV technique was applied to measure the recombination lifetime (τ_{rec}) of charge carriers as well as the total carrier concentration (n) in devices. We measured the TPV at the open-circuit condition over a range of different light intensity. When the device output reached a steady state, pulsed laser which generates the small perturbation was applied. Because no charge is collected at the open-circuit condition, excess charge carriers generated layer by the pulsed laser are recombined with recombination lifetime (τ_{rec}) at P3HT/PCBM interfaces and/or P3HT:PCBM/Al interfaces, resulting in the decay of the photovoltage. We assert that the recombination process of devices in this study is predominantly influenced by the non-geminate recombination at the active layer/Al, not by the geminate recombination, because we used active layers with the same bulk morphology regarding the devices with and without the TNL. It has been reported that non-geminate recombination is closely related to the V_{OC}, while geminate recombination is mainly related with the free charge carrier creation, which can affect the photocurrent [26–29]. Fig. 3a shows typical law data of measured TPV (at 1 sun illumination condition). The τ_{rec} can be obtained by fitting the TPV to mono-exponential decay function [19,30]. In order to make an equitable comparison of the carrier recombination dynamics, the total carrier concentration in a device at the open-circuit condition under a steady-state illumination was estimated by a differential charging method using the TPV and TPC measurements [19]. Charge carrier density generated inside the devices was obtained by integrating C with respect to voltage (Eq. (1)).

$$n = \frac{1}{Aed}\int_0^{V_{OC}} C dV \tag{1}$$

where A is the device area, e is electronic charge, d is the device thickness, and C is the capacitance.

The differential capacitance C is defined as the voltage change when a small amount of charge is added to the device.

$$C = \Delta Q/\Delta V_0 \tag{2}$$

ΔQ can be obtained by integrating with respect to time the short-circuit photocurrent transient for the same laser pulse (Fig. 3b). C is found to increase exponentially with increasing V_{OC}, which was extrapolated back to $V = 0$.

Fig. 3c shows the carrier concentration as a function of light intensity for the devices with and without the TNL. The carrier concentration of the device with the TNL was higher than that of the device without the TNL under the same light intensity as can be seen in Fig. 3c. In general, a higher carrier concentration can be caused by elongated recombination lifetime and/or by an increased photogeneration of charge carriers. TiO_x and ZnO are well known as an optical spacer [13,31]. The TiO_2 interfacial layer also worked as an optical spacer. However, the significant enhancement of J_{SC} by the optical the photocurrent enhancement by the

Table 1
The photovoltaic parameters obtained from *J–V* curves of P3HT:PCBM devices.

Devices	J_{SC} (mA/cm^2)	V_{OC} (V)	*FF*	PCE (%)	R_{sh} (kΩ cm^2)	R_s (Ω cm^2)	*n*	J_0 (mA/cm^2)
Pre-annealed/Al	8.61	0.48	0.47	1.93	70	14.3	1.71	1.32×10^{-6}
Post-annealed/Al	9.63	0.62	0.64	3.78	574	10.5	2.11	5.63×10^{-8}
Pre-annealed/TNL/Al	8.64	0.60	0.63	3.30	143	14.1	1.78	7.56×10^{-8}
DIO/Al	8.83	0.46	0.52	2.13	127	18.3	1.89	1.52×10^{-6}
DIO/TNL/Al	9.66	0.62	0.66	3.95	392	13.2	1.86	3.36×10^{-8}

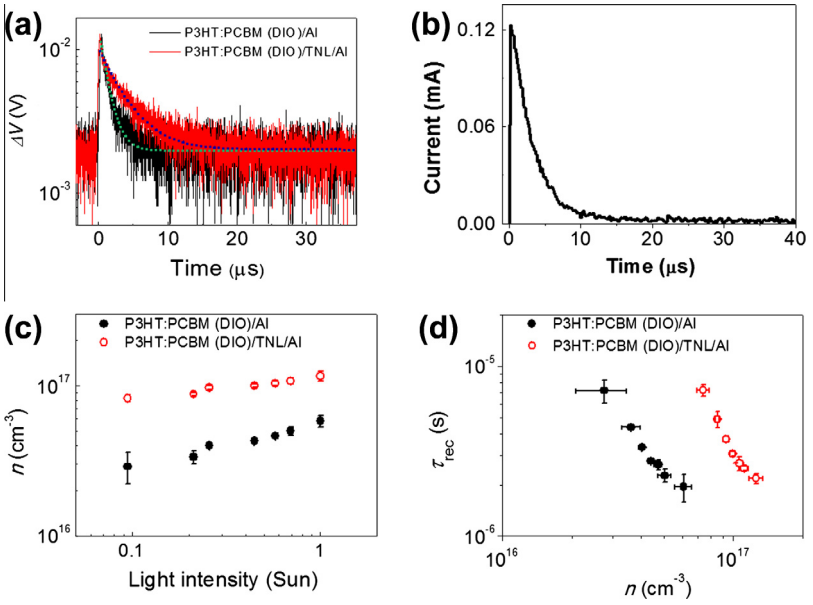

Fig. 3. (a) TPV measured at 1 sun light intensity. The dotted lines are mono-exponential decay curve fits. (b) Transient photocurrent measured under 1 sun light intensity using the same intensity laser pulse as (a). (c) Charge carrier concentration versus light intensity. (d) Recombination lifetime versus charge carrier concentration for the DIO-processed P3HT:PCBM device with and without the TNL.

optical spacer was not observed (Fig. 4). As shown in the reflective mode absorption results, change in the optical absorption of the active layer according to insertion of the TNL is insignificant. The efficacy of optical spacer is correlated with the surface roughness of active layer. It has been reported that the efficacy of optical spacer can become diminished when the surface roughness of active layer is increased [14]. It was found that the RMS roughness of the active layer was increased from 1 nm to 9 nm after processing with DIO as a processing additive (Fig. 4). Thus, it is thought that J_{SC} enhancement by the optical spacer effect of the TiO_2 layer is not significant in our devices.

The τ_{rec} are plotted as a function of the charge carrier concentration (Fig. 3d). The τ_{rec} of the device with the TNL was significantly extended in comparison to the device without the TNL at the equivalent carrier concentration. This result indicates that the TNL effectively suppressed the non-geminate recombination at the active layer/TiO_2 interfaces and enhanced recombination lifetime, resulting in an increase of carrier concentration at the active layer. In other words, the increased carrier concentration might elevate the difference of the quasi-fermi levels between holes in P3HT and electrons in PCBM and this result can account for the enhanced V_{OC}.

To investigate the effect of the TNL as a hole blocker on the enhanced diode property and V_{OC} of the devices, we analyzed the dark current characteristics as shown in Fig. 5a and b using the equivalent circuit model and the following equation [32]:

$$J = J_0\left\{\exp\left[\frac{q(V - JAR_s)}{nkT}\right] - 1\right\} + \frac{V - JAR_s}{AR_{sh}} - J_{ph}(V), \qquad (3)$$

where J_0, q, n, R_s, R_{sh}, k, T, and A is reverse saturation current density, elementary charge, ideality factor, series resistance, shunt resistance, Boltzmann constant, absolute temperature, and the active area of the device. The parameters related with the diode properties (J_0,n) are summarized in Table 1. J_0 and n were obtained by fitting dark *J–V* curves for the positive bias region according to modified Shockley equation expressed as $\ln[J - (V - JAR_s)/AR_{sh}] = \ln J_0 + [-q(V - JAR_s)/nkT]$. The J_0 has a physical meaning for the number of injected charges which can overcome the energy barrier under the reverse bias and the J_0 value is closely related with the V_{OC} value [22,24,33]. Assuming infinite shunt resistance and infinitesimal series resistance, the Shockley equation can be simplified as the following form under the open-circuit condition [24]:

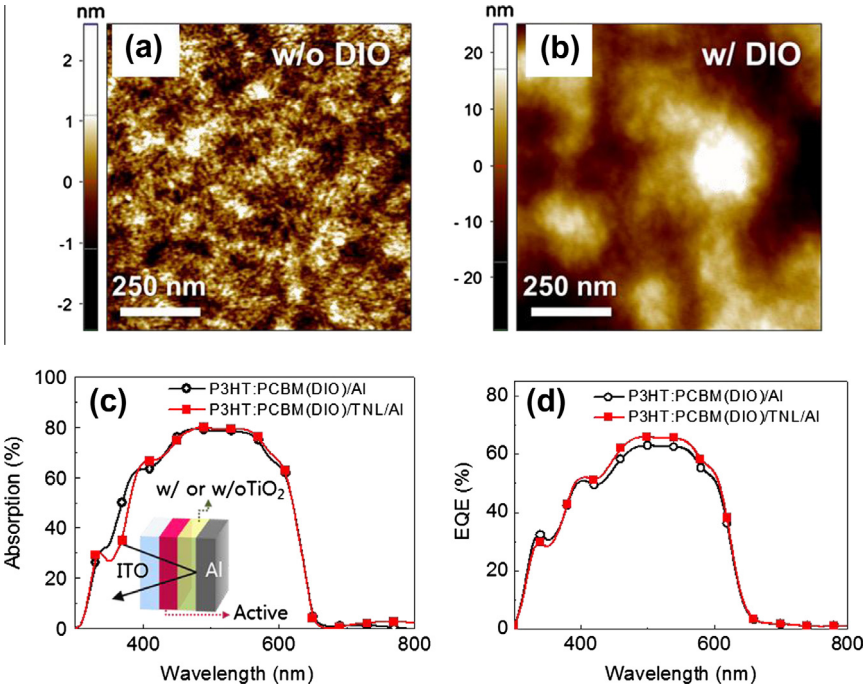

Fig. 4. Atomic force microscope image of P3HT:PCBM film (a) without additive, (b) with additive, (c) refractive mode absorption spectra and (d) EQE spectra for DIO-processed devices with and without the TNL.

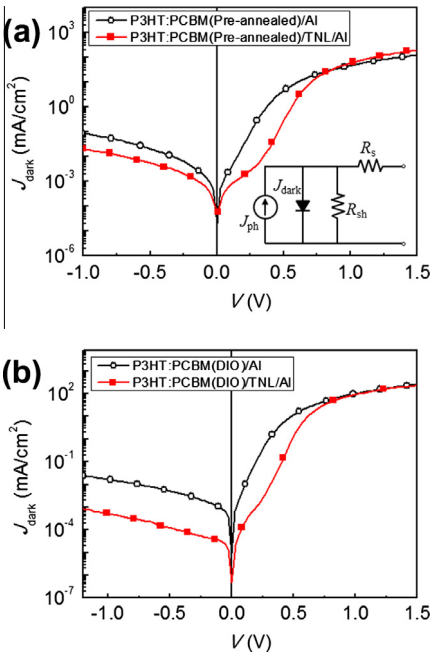

Fig. 5. *J*–*V* curves of thermally-annealed (a) and DIO-processed (b) P3HT:PCBM devices measured in the dark. An inset in (a) is the equivalent circuit diagram.

$$V_{OC} = \frac{nkT}{q} \ln\left[\frac{J_{ph}(V_{OC})}{J_0} + 1\right] \approx \frac{nkT}{q} \ln\left[\frac{J_{ph}(V_{OC})}{J_0}\right], \qquad (4)$$

where J_{ph} (V_{OC}) is the photocurrent at V_{OC}. This equation implies that V_{OC} is dependent upon n, J_{ph} (V_{OC}), and J_0 at the same temperature. Since there were few differences in the n between the device with and without the TNL, the increased V_{OC} in the devices with the TNL was directly correlated with the decreased J_0 value. For the devices with and without the TNL, the variation of J_{ph} (V_{OC}) was negligible compared to that of the J_0. Thus, reduced V_{OC} values observed in pre-annealed and DIO-processed devices without the TNL can be explained by the higher J_0 due to large injection leakage, which resulted from surface-segregated P3HT phase. On the other hand, a relatively low J_0 was observed in devices with the TNL. For the pre-annealed and DIO-processed devices, the use of the TNL with a deep valence band prevented the hole leakage between the P3HT phase and the Al electrode. Consequently, the TNL effectively decreased the J_0 and enhanced the diode character, resulting in the improvement of V_{OC} and *FF*.

To demonstrate technical advantages of TNL, we fabricated an annealing-free flexible device with DIO and TNL. The insertion of the TNL into the DIO-processed device (annealing-free process) enabled us to fabricate efficient flexible PSC devices on the plastic substrate since this method was solution-processable at room temperature. The *J*–*V* characteristics of the thermally annealed device and the annealing-free device fabricated on ITO/PEN (poly ethylene naphthalate) substrate are shown in Fig. 6a. The annealing-free device with DIO and TNL yielded the better performance (V_{OC} = 0.58 V, J_{sc} = 7.89 mA cm^{-2}, *FF* = 0.60, and PCE = 2.75%) compared to that of the thermally annealed device (V_{OC} = 0.59 V, J_{sc} = 7.44 mA cm^{-2}, *FF* = 0.40, and PCE = 1.74%). Furthermore, the device using TNL presented enhanced air stability as compared with the device using the Ca/Al electrode. The PCE of the device with the

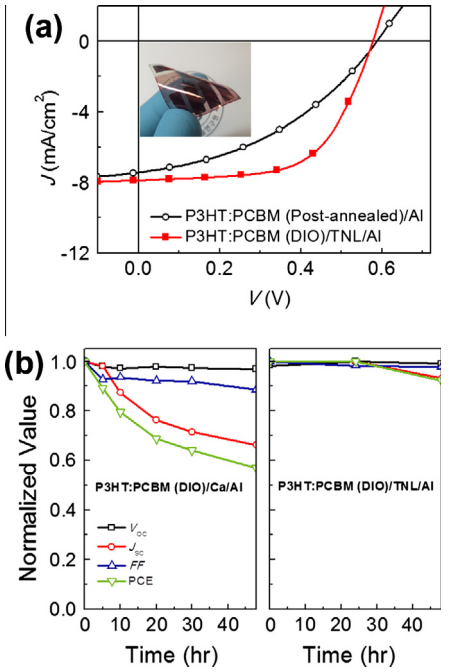

Fig. 6. (a) *J–V* curves of the post-annealed and DIO-processed P3HT:PCBM devices fabricated on flexible ITO PEN substrates. (b) Air stability of DIO-processed devices with the Ca/Al and TNL/Al electrodes in the dark.

Ca/Al electrode was decreased to 56% of the initial PCE after 48 h, while the device with TNL maintained 92% of the initial PCE during the same period in the dark (Fig. 6b). It is reported that the TiO_x inter-layer protects the active layer from physical or chemical interaction with the Al electrode as well as prevents the permeation of oxygen and moisture into the active layer, resulting in enhanced the air stability of solar cells. It is thought that the TiO_2 nanoparticle inter-layer (TNL) used in this experiment enhance the solar cell efficiency in the same way [34].

4. Conclusions

We have demonstrated the effect of the TiO_2 nanoparticle interfacial layer on photovoltaic properties. Although the processing additive provides an efficient way to control the bulk morphology in PSCs, the device showed the reduced V_{OC} due to the undesirable surface compositions of P3HT:PCBM at the active layer/Al interface. The deteriorated photovoltaic performances can be resolved by introducing the TNL. The TNL effectively suppresses the leakage current and recombination near the active/Al interface for devices possessing unfavorable surface composition. The device with DIO and TNL shows outstanding performance on the flexible substrate (2.75%) as well as the glass substrate (3.95%).

Acknowledgements

This research was supported by the Pioneer Research Center Program through the National Research Foundation of Korea funded by the Ministry of Education, Science and Technology (2008-2000092), by the Global Frontier R&D Program on Center for Multiscale Energy System funded by the National Research Foundation under the Ministry of Education and by KRCF (Korea Research Council of Fundamental Science &Science and Technology and Technology) and KIST (Korea Institute of Science & Technology) for"NAP (National Agenda Project) program".

References

[1] K.X. Steirer, J.J. Berry, M.O. Reese, M.F.A.M. van Hest, A. Miedaner, M.W. Liberatore, R.T. Collins, D.S. Ginley, Thin Solid Films 517 (2009) 2781.
[2] S.E. Shaheen, R. Radspinner, N. Peyghambarian, G.E. Jabbour, Appl. Phys. Lett. 79 (2001) 2996.
[3] F.C. Krebs, S.A. Gevorgyan, J. Alstrup, J. Mater. Chem. 19 (2009) 5442.
[4] J. Peet, J. Kim, N.E. Coates, W.L. Ma, D. Moses, A.J. Heeger, G.C. Bazan, Nat. Mater. 6 (2007) 497.
[5] J.K. Lee, W.L. Ma, C.J. Brabec, J. Yuen, J.S. Moon, J.Y. Kim, K. Lee, G.C. Bazan, A.J. Heeger, J. Am. Chem. Soc. 130 (2008) 3619.
[6] J. Liu, S. Shao, H. Wang, K. Zhao, L. Xue, X. Gao, Z. Xie, Y. Han, Org. Electron. 11 (2010) 775.
[7] M.S. Su, C.Y. Kuo, M.C. Yuan, U.S. Jeng, C.J. Su, K.H. Wei, Adv. Mater. 23 (2011) 3315.
[8] G. Li, V. Shrotriya, J.S. Huang, Y. Yao, T. Moriarty, K. Emery, Y. Yang, Nat. Mater. 4 (2005) 864.
[9] K.M.A.J. Moulé, Adv. Mater. 20 (2008) 240.
[10] J. Ouyang, Y. Xia, Sol. Energy Mater. Sol. Cells 93 (2009) 1592.
[11] Y. Yao, J. Hou, Z. Xu, G. Li, Y. Yang, Adv. Funct. Mater. 18 (2008) 1783.
[12] S.J. Lou, J.M. Szarko, T. Xu, L. Yu, T.J. Marks, L.X. Chen, J. Am. Chem. Soc. 133 (2011) 20661.
[13] Y. Liang, Z. Xu, J.B. Xia, S.T. Tsai, Y. Wu, G. Li, C. Ray, L.P. Yu, Adv. Mater. 22 (2010) E135.
[14] J.Y. Kim, S.H. Kim, H.-H. Lee, K. Lee, W. Ma, X. Gong, A.J. Heeger, Adv. Mater. 18 (2006) 572.
[15] J.K. Lee, N.E. Coates, S. Cho, N.S. Cho, D. Moses, G.C. Bazan, K. Lee, A.J. Heeger, Appl. Phys. Lett. 92 (2008) 243308.
[16] W.S. Chung, H. Lee, W. Lee, M.J. Ko, N.G. Park, B.K. Ju, K. Kim, Org. Electron. 11 (2010) 521.
[17] T. Kim, J.H. Jeon, S. Han, D.K. Lee, H. Kim, W. Lee, K. Kim, Appl. Phys. Lett. 98 (2011) 183503.
[18] E. Scolan, C. Sanchez, Chem. Mater. 10 (1998) 3217.
[19] C. Shuttle, B. O' Regan, A. Ballantyne, J. Nelson, D. Bradley, J. de Mello, J. Durrant, Appl. Phys. Lett. 92 (2008) 093311.
[20] X. Wang, T. Ederth, O. Inganas, Langmuir 22 (2006) 9287.
[21] C.M. Bjorstrom, S. Nilsson, A. Bernasik, A. Budkowski, M. Andersson, K.O. Magnusson, E. Moons, Appl. Surf. Sci. 253 (2007) 3906.
[22] A. Orimo, K. Masuda, S. Honda, H. Benten, S. Ito, H. Ohkita, H. Tsuji, Appl. Phys. Lett. 96 (2010) 043305.
[23] D. Chen, A. Nakahara, D. Wei, D. Nordlund, T.P. Russell, Nano Lett. 11 (2011) 561.
[24] J.H. Lee, S. Cho, A. Roy, H.T. Jung, A.J. Heeger, Appl. Phys. Lett. 96 (2010) 163303.
[25] A. Hayakawa, O. Yoshikawa, T. Fujieda, K. Uehara, S. Yoshikawa, Appl. Phys. Lett. 90 (2007) 163517.
[26] A. Maurano, R. Hamilton, C.G. Shuttle, A.M. Ballantyne, J. Nelson, B. O' Regan, W. Zhang, I. McCulloch, H. Azimi, M. Morana, Adv. Mater. 22 (2010) 4987.
[27] S.K. Pal, T. Kesti, M. Maiti, F. Zhang, O. Inganas, S. Hellstro m, M.R. Andersson, F. Oswald, F. Langa, T.O. Sterman, J. Am. Chem. Soc. 132 (2010) 12440.
[28] K. Maturova, S.S. van Bavel, M.M. Wienk, R.A.J. Janssen, M. Kemerink, Adv. Funct. Mater. 21 (2011) 261.
[29] D. Credgington, R. Hamilton, P. Atienzar, J. Nelson, J.R. Durrant, Adv. Funct. Mater. 21 (2011) 2744.
[30] R. Hamilton, C.G. Shuttle, B. O' Regan, T.C. Hammant, J. Nelson, J.R. Durrant, J. Phys. Chem. Lett. 1 (2010) 1432.
[31] J. Gilot, I. Barbu, M.M. Wienk, R.A.J. Janssen, Appl. Phys. Lett. 91 (2007) 11350.
[32] S.M. Sze, K.K. Ng, Physics of Semiconductor Devices, Wiley-Blackwell, 2007.
[33] C. Waldauf, M.C. Scharber, P. Schilinsky, J.A. Hauch, C.J. Brabec, J. Appl. Phys. 99 (2006) 104503.
[34] K. Lee, J.Y. Kim, S.H. Park, S.H. Kim, S. Cho, A.J. Heeger, Adv. Mater. 19 (2007) 2445.